ISROMAC-11 Proceedings of the International Symposium on
Transport Phenomena and Dynamics of Rotating Machinery,
Feb.26-March 2, 2006, Honolulu, Hawaii, USA

Flow around Helicopter Blade Tip Sections Using a (3d) Stereoscopic Particle Image Velocimeter - Part II

Harika S Kahveci[1] & Cengiz Camci[2]
Turbomachinery Aero-Heat Transfer Laboratory
The Pennsylvania State University
223 Hammond Building, University Park, PA 16802
814 865 9871 fax : 814 865 7092

ABSTRACT

The present investigation deals with the detailed aerodynamic flow near a rotating helicopter rotor blade. Three-component velocity measurements using a Stereoscopic Particle Image Velocimetry system reveal the details of the near tip flow at various blade angle-of-attack values. The instantaneous flow in selected planes that are almost normal to the rotor blade tips is measured in a phase-locked manner as observed from the stationary frame. A model helicopter with a two-bladed rotor is utilized for experiments at a speed of 570 rpm corresponding to a tip velocity of 35.8 m/s (117.5 ft/s) and a tip Reynolds number of 9.6×10^4. Radial motion along the blade is analyzed with 3D PIV. Aerodynamic results obtained near the tip region, and specific issues related to the 3D PIV technique are discussed in detail. The current PIV results effectively show fine details of highly 3D flow fields near rotating machinery components.

INTRODUCTION

PIV technique provides instantaneous velocity information over a whole flow field, and hence it is advantageous to use this technique for instantaneous and unsteady/turbulent flow events such as flows in wind turbine blades, jets, and rotor blades. Its superior features such as higher accuracy, higher speed, and its ability to perform planar measurements are the reasons why this technique is preferred and used throughout this study at Penn State University.

Laser techniques are preferred in flow field investigations because of their reliability, speed, and non-intrusive characteristic. Besides all of these, PIV, which is a planar measurement technique, is also capable of detecting unsteady flow phenomena and instantaneous velocities, even in a phase-locked arrangement. The study of Lang et al [1] is a good example of 3D PIV application in an axial transonic turbine. They investigated the flow at different stator-rotor positions, and observed the vortex shedding in the rotor. 3D PIV was also used to obtain the detailed flow characteristics within a screeching cycle. In their research, Alkislar et al [2] used novel mesh-free and high resolution approaches to measure supersonic flow.

The principles of 3D PIV were applied to the flow around a Rushton turbine by Hill et al [3], which was a suitable testing ground for three-dimensionality of the flow field. It was observed that the radial jet and blade tip vortices were responsible for the large-scale circulation. Funes-Gallanzi et al [4] made measurements in the wake region of an unsteady transonic flow using 3D PIV, and verified the results with 3D computations.

After 2D PIV measurements were performed at the Turbomachinery Heat Transfer Laboratory by Uzol [5], and Uzol and Camci [6] on gas turbine blade cooling applications, the use of 3D PIV technique for experimental purposes has been recently initiated in order to investigate the three dimensional flows in turbomachinery systems. The most recent research was done at the downstream of a rotor in an axial flow turbine in order to investigate the stage exit flow, Tajiri [7] .

This research makes use of 3D PIV to investigate three dimensional flow characteristics near helicopter blades. Although several detailed studies in rotor wakes have been performed so far using LDV by Leishman et al [10,11,12], not as many have been reported using a 3D PIV for rotor wake investigations.

Flow Around Helicopter Rotor Blades: The flow is unsteady due to blade boundary layers, vortex shedding especially at high angle of attack. The flexible motion of the rotor blades (such as pitch etc.) also makes the secondary

1 Graduate Res. Asst. , presently at GE Power Systems, Greenville, SC
2 Professor of Aerospace Engineering, (cxc11@psu.edu)

flows and tip vortices more difficult to understand compared to flow around the antenna.

During the rotation of the helicopter blades, vortices created at blade tips have a strong effect on the overall rotor flow field. This effect dominates for many rotations, which has a consecutive effect on aerodynamic loading of blades. For a maneuvering helicopter, the rotor performance and dynamics are further affected, and this phenomenon is called 'blade vortex interaction, (BVI)'. This interaction introduces more airloads acting on the blades, and results in an increased noise generation. Therefore, the flow characteristics around helicopter blades need to be investigated to have a better understanding of how the rotor performance, acoustics, and loads are affected during the flight.

There have been many studies performed to investigate the flow characteristics of rotor blades. First studies were carried out by using hot-wires or pressure probes. Wind tunnels have been utilized to measure the rotor blade pressures during flight. Lorber [8] used a pressure-instrumented helicopter model under level, hover, and descent conditions, and obtained several measurements for blade pressures and wake interactions by wind tunnel testing. It was observed that the BVI events were repeatable and consistent.

In order to understand the flow field and noise-generating mechanisms, some computational codes were developed as well. Within an international cooperative program, a helicopter model was tested in the German Dutch Wind Tunnel (DNW), and the data was compared with numerical methods developed by DLR of Germany, ONERA of France, and the Aeroflightdynamics Directorate (AFDD) of the U.S. Army [9]. Blade surface pressures, vortex core size and trajectories were examined. It was concluded that in order to improve the prediction capabilities, more experimental data is needed for detailed wake information.

Limitations of experimental work such as flow disturbance by probes, and unresolved time-dependent nature of the flow were overcome by the introduction of laser techniques in flow field investigations. Leishman et al [10-14] have performed many studies using three-dimensional Laser Doppler Velocimetry technique. In these studies, three-dimensional velocity field, circulation profiles, aperiodicity effects, and turbulence quantities were investigated for single and two-bladed rotors.

Besides LDV studies, 2D PIV has also been applied for rotor analysis so far. Raffel et al [15] measured blade tip vortices by utilizing both LDV and 2D PIV techniques. The both techniques were compared for the first time using the same rotor in a wind tunnel. The recording of the PIV images were performed phase-locked with the rotor motion. It was observed that the results obtained were similar, with the advantage of less time needed by PIV technique.

For rotating flow fields, PIV is found to be more efficient to be used over large areas. A variation of 2D PIV was developed and applied to a flow field generated by a four-bladed helicopter rotor by Saripalli et al [16]. The velocity and vorticity measurements were made and compared with other published data. A Blade-Vortex Interaction (BVI) study with secondary vertical structures investigation was performed over a single-blade rotor disk by Horner et al [17]. A stationary wing was subjected to an oncoming vortex generated upstream of the rotor disk, and the data for different azimuth angles were compared.

Since 3D PIV is a relatively new technique compared to 2D PIV, there have been only a few studies with its application in this field so far.

A very similar study to this research was realized by Heineck et al [18] using 3D PIV in order to obtain the instantaneous vortex locations of a two-bladed rotor in hover. Very recent 3D PIV measurements were performed by Burley et al [19] for vortex analysis within the wake across a rotor disk plane. The determination of vortex parameters is important for Blade Vortex Interaction, BVI.

In addition, it should be noted that there is only a single camera capturing the images in traditional 2D PIV, where the out-of-plane is lost because of the projection of the vectors into the light sheet. In 3D PIV, there is an additional camera viewing the field from a different angle. The two-dimensional image obtained by each camera is different than that of the other, and they are afterwards combined to give three-dimensional velocity information.

For 3D analysis, the 2D calibration images need additionally to be converted into 3D data by a Direct Linear Transform (DLT) model, in order to calculate the third component of the velocity. Correlation techniques are used to obtain raw vector maps out of image pairs taken during experiments, and some calculation methods are used to evaluate these vector maps afterwards. In the 3D part of this research, two of the 80C60 HiSense PIV/PLIF cameras with 1024 x 1280 pixels are used with 80N57 Personality Module fitted to processor, and a Nikon Micro-Nikkor 60/2.8 objective, for each.

TEST SETUP

The same helicopter model is used as in Part-I. Experiments are performed on a section of the blade at 5 cm (1.97 in) distance from the tip (measured radially inward from the tip), and at 3 cm (1.18 in) in front of the blade tip (no blade interference). For each location, flow field in the effect of -5º, 0º, 5º, and 10º pitch is presented. The laser thickness is taken to be 6 mm (0.24 in) as in Part-I, and is applied right after 3 cm (1.18 in) and 5 cm (1.97 in) distances. The distances are exaggerated in Fig. 1 for clarity.

The measurements are this time performed with 3D PIV. The system is the same as in Part-I, except an additional camera of the same model. However, the test setup differs from that of 2D PIV application. As is used for the 3D jet flow analysis, the two cameras are mounted on a

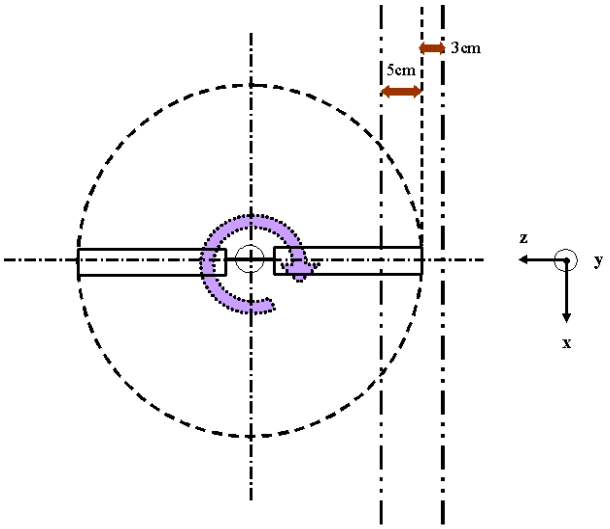

Figure 1. Laser sheet locations on the helicopter blade for 3D analysis

traverse plate such that the laser and the cameras all tied to the same frame of reference. The traverse plate is horizontal this time, to provide the vertical laser sheet in the flow field. The cameras are oriented at an angle to the plane of the light sheet as to capture the possible largest view of the field of interest.

The experiments are run in phase-locked condition with applying some trigger delay to capture the image of the blade at the same location throughout different measurements. This location is (20mm, 0mm) (0.79in, 0in) coordinates on the target plate which is determined for zero pitch condition. To obtain this fixed blade location, the setup of the previous experiments with single camera is used. The camera is placed at a distance in front of the blade to be able to capture the motion of the blade when it is parallel to the camera plane. The trigger delay is applied accordingly to satisfy this condition. Afterwards, the 3D test setup is used with the same trigger delay. Although the cameras view the flow field at an angle and do not capture the blade cross section, the actual location of the blade on the overlapped 3D vector map is known. The trigger delay depends on the velocity of the rotor. All experiments are performed with the same tip velocity (or rpm), therefore keeping the trigger delay the same.

Since the locations of the cameras are fixed on the same traverse plate with the laser, performing the calibration only once is enough for all experiments. Therefore, the level of the camera is kept the same each time, which also provides a comparison of the blade locations with different pitches for these 3D experiments. The vertical position of blade tip cross section may vary when blade pitch angle is varied. This is because of a different thrust magnitude and direction which may occur at different pitch angle settings.

The camera device type has been selected as HiSense Type 13[gainx4] so far. For 3D PIV analysis, the device type has been selected as HiSense 8-bit reduction (type 13) gain x 4.

The cameras see the flow field at an angle as shown in Fig. 2. The speckle images shown in Figs. 3 and 4 are taken during a stereoscopic -5º pitch experiment. The reflection of the laser sheet where it cuts the blade at 5 cm (1.97 in) section can be seen from both cameras. The actual field of interest is the area that will be formed by the overlap of these two images. Overlapping is applied after the vector maps are obtained by adaptive-correlation out of these speckle images. It should be noted that the cross section can not be observed with true geometry, here. But, it is already known to be located parallel to the plane where the overlapping region of the two cameras coincide with, via the test setup procedure followed. Hence, with the same trigger delay, the blade is viewed as follows at 5 cm (1.97 in) section.

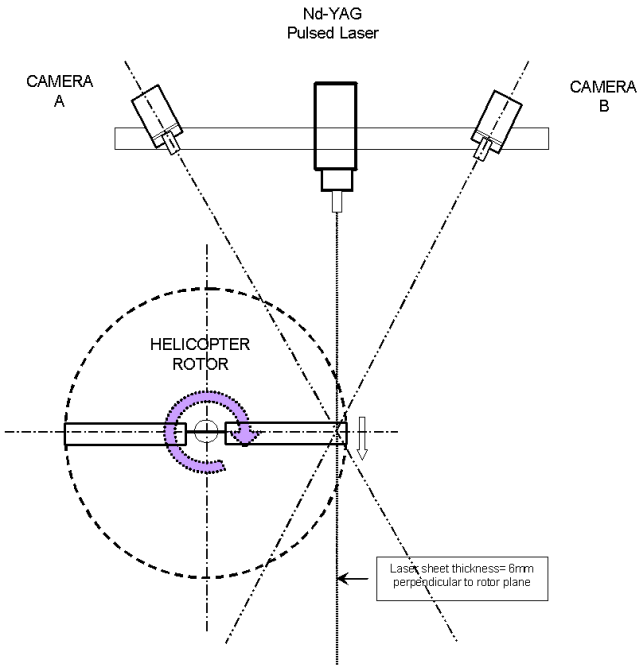

Figure 2. 3D PIV setup for helicopter experiments

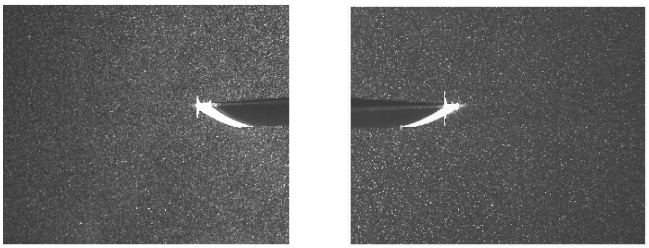

Figure 3. Images captured by the cameras during the experiment

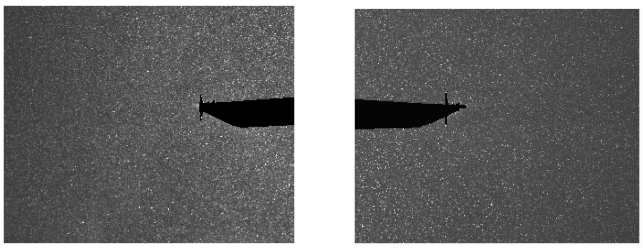

Figure 4. Masked flow field images

The reflection and the blade are masked in the images to avoid any interference possible with the flow. The images obtained by the cameras are later processed with adaptive-correlation with a 16x16 interrogation area and 50% overlap. The peak validation coefficient is taken as 1.1.

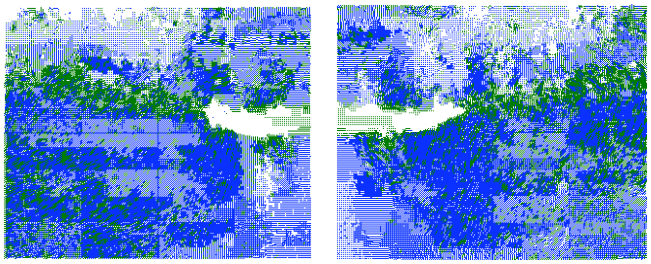

Figure 5. Instantaneous vector maps obtained by adaptive-correlation

The vector maps obtained as a result of correlation procedure are shown in Fig. 5. The region of masking is clear. Although, this part of blade does not exist on the third plane of overlapping region, which is the actual field of interest, it still affects the flow field taken by each camera due to its existence. This can also be observed in 3D vector maps. Therefore, masking is necessary.

EXPERIMENTAL RESULTS AND DISCUSSIONS

5 cm (1.97 in) Away From the Tip: -5º Pitch: Every 3 vectors out of 4 in x-direction, and every 6 vectors out of 7 in y-direction are cancelled for clarity of vector representation. The difference of the maps presented in this chapter is that these maps give all velocity components in three directions, the colored contours being the magnitude of the third velocity component, W (out of plane component). Positive values of W are defined as out of page, whereas negative values show that the direction is into the page.

The airfoil cross section is parallel to the laser sheet plane at this location, that is, the blade extends out of the page in the same direction with positive W components. Although the direction of the rotor rotation is the same with that of 2D PIV experiments, the camera setup has changed. This results in a reversed x-axis in the following maps, where the laser sheet generation and the airfoil motion are from left to right this time. The magnitudes of the vector components in x- and y-directions can be determined with a comparison with the reference vector given on each map.

In Fig. 6, the light blue region close to airfoil corresponds to the masked region in the flow field images due to the existence of the blade. The velocity is zero across this region in all directions.

During the test setup, the blade is located so that it lies at a 20 mm (0.79 in) distance from the origin in x-direction.

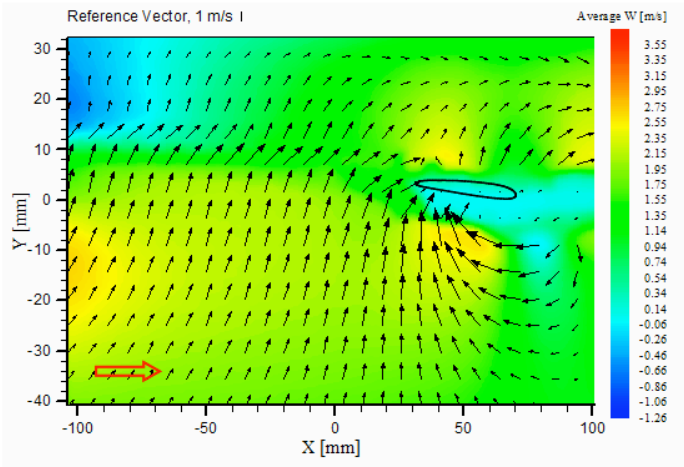

Figure 6. 3D vector map with colored contours at -5º pitch 5 cm (1.97 in) away from the tip

But, it appears to be that there is around a 10 mm (0.4 in) shift in this direction when flow characteristics are examined. This introduces the need of a better technique to identify the exact location of the blade for stereoscopic measurements. This difference may be due to slight variations in the velocity during the experiment, which changes trigger delay, and hence the location of the airfoil. If an analog time delay device is used instead of software imposed delay, a continuous adjustment of blade position may be possible.

When compared with the previously obtained maps, the negative pitch has the same effect on the flow field as it was observed before. There is an upwash in the whole flow field. The flow is deflected away by the motion of leading edge, and it moves towards trailing edge on the lower surface. The U and V components of velocity have their highest values on the lower surface where there is a re-circulatory flow pattern. The trace of trailing edge affects the flow behind, having the flow to have high magnitude as well.

The W component of flow shows the radial components created by the blade rotation. There is a vorticity that can be observed by the lower surface of the airfoil. In a region between the trailing edge up to the leading edge, flow moves towards the center of the rotor. By the leading edge it

changes direction, and moves in the opposite direction away from the center. The motion towards the center is more significant, when the magnitudes are compared from the scale. On the upper surface, flow moves only in one direction, towards the center along the blade, the similar regions for lower surface having a higher magnitude.

At the far back of aft point, again another vorticity can be observed. This motion has the trajectory of the airfoil as a symmetry axis. Above this path, the airfoil deflects the flow away from the blade. Motion is towards the center below.

0º Pitch: When compared to other pitch angles, there is a significant decrease in magnitudes of velocity in all directions as observed in Fig. 7. The airfoil boundary layers at zero pitch are fully attached. Due to the 'almost' symmetrical airfoil shape, the lift production is minimal. The wake of the airfoil is almost negligible.

There is symmetry between the characteristics of the flow on the lower and the upper surfaces, as it is found in 2D experiments. The flow follows the airfoil behind. There are two slight vorticities on each surface starting somewhere in front of the airfoil moving towards the trailing edge. Across the chord, the radial motion is towards the center, and more significant as for the negative pitch case. In the region at the front of the airfoil, flow moves away in the opposite direction.

A clear wake region behind the airfoil is observed. This section has a slightly higher magnitude for W (radially outward) component. In the upper part of the wake region, the U components are almost horizontal and relatively large, but W components are small than that of the lower region.

As it is explained before, the original location of the stationary blade at zero pitch condition is (20mm, 0mm) (0.79in, 0in) point. The airfoil's position during the experiment is found to be at (30mm ,8mm) (1.18in, 0.31in).

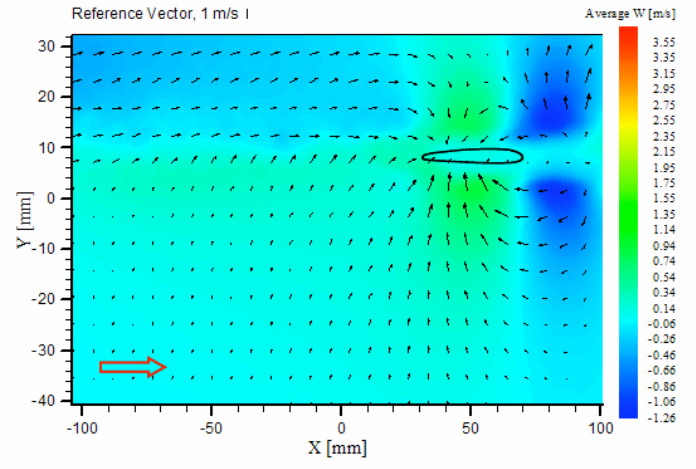

Figure 7. 3D vector map with colored contours at 0º pitch 5 cm (1.97 in) away from the tip

A slight uncertainty in the trigger delay might cause a shift of 10 mm (0.4 in) in horizontal direction. Even the lift production is minimal, there is a slight upward motion of the blade. As the blade rotates, the blades move upwards. For negative pitch case, the airfoil appears to be at around Y=0. The airfoil will be found at a higher location in the upcoming experiment, that is for positive pitch angle. The elastic motion is affected by the amount and the direction of the pitch due to the upwash and downwash phenomena.

5º Pitch: The light blue region close to airfoil in Fig. 8 corresponds to the masked region. The airfoil is found to be located at around 15 mm (0.59 in) height. A vorticity zone near the upper surface of the airfoil, and a general downwash behavior in the flow field are obvious as general characteristics of a positive pitch case. There is no significant recirculation observed on the lower surface; instead the flow is deflected away in different directions.

The ground effect, which is observed in 2D PIV experiment for the same location and pitch, is observed here as well, reflecting the flow away almost at the same level below the airfoil surface.

The motion on the upper part of the flow field is more distinct compared to the lower part. Flow in 5º pitch shows almost a mirror image behavior of -5º pitch case. The radial components verify this, too. The only difference is that the opposite motion in radial direction on the upper surface of the airfoil has higher magnitudes. If the cameras could view a larger section of the field, the blue region on the top left of -5º pitch map would continue to the right as to create a mirror image of the map above.

10º Pitch: Figure 9 shows the experiment results corresponding to the highest positive pitch. Downwash character is more effective over the flow field, hence more

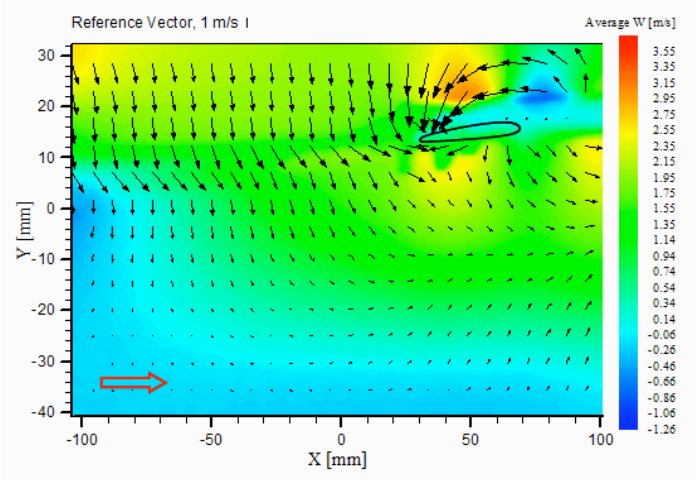

Figure 8. 3D vector map with colored contours at 5º pitch 5 cm (1.97 in) away from the tip

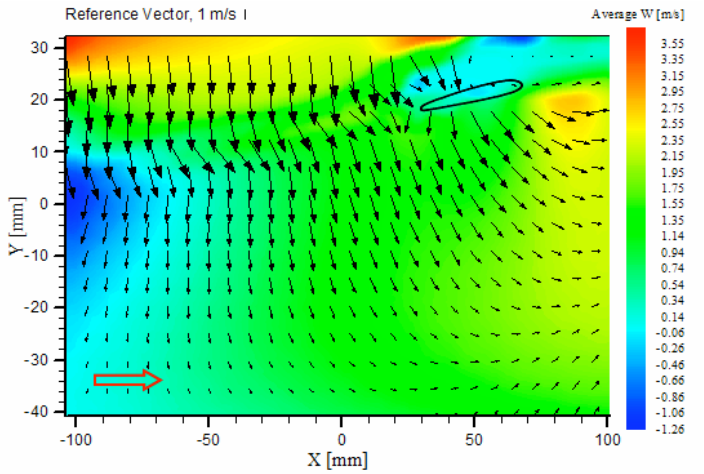

Figure 9. 3D vector map with colored contours at 10º pitch 5 cm (1.97 in) away from the tip

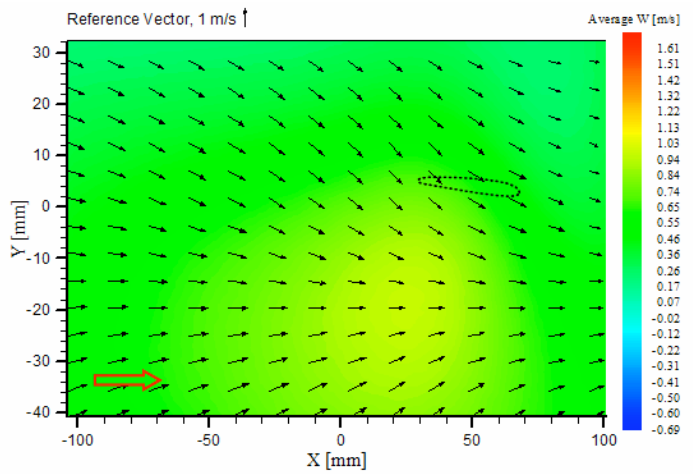

Figure 10. 3D vector map with colored contours at -5º pitch 3 cm (1.18 in) in front of the tip

lift is produced. As a result of significant lift, the location of the airfoil is in an upper level around 20 mm (0.79 in). The difference between the magnitudes of radial component is more severe. There is an expected vorticity to take place on the upper surface of the airfoil, but PIV measurement area is not large enough to include it. As for the previous positive pitch case, the flow is reflected from the ground. Since the lift produced by the airfoil is higher, the downwash behavior is much stronger. As a result, the ground effect is reduced, and the flow turns its direction upwards at a lower level.

3 cm (1.18 in) In Front of the Tip: In this section, the flow field in the vicinity of the blade tip is investigated. The near tip flow influence is documented in this region. The cameras look at the flow field at an angle, but the blade existence in the images is not very significant. At the time of image acquisition, the blades are not in the laser sheet. Although the whole speckle image is available for PIV correlation, there is still a faded background image of blade in each frame. Since the background of the blade image is out of focus, velocity vectors are still available in that region. Therefore, masking is not applied.

-5º Pitch: Since the airfoil tip is not in the laser sheet plane, its relative position with respect to the measurement location is shown with a dashed airfoil contour in Fig. 10. The near tip flow does not have a strong 3D appearance at 3 cm (1.18 in) in front of the tip. This is because the airfoil is small in size, and the velocity of the rotor is not high enough to be able to affect the flow in the vicinity of the airfoil. Apparent horizontal components in +X direction are because of the viscous shear imposed by the airfoil tip section.

0º Pitch: The flow near the tip follows the blade in general as shown in Fig. 11. The U and V velocity components have higher magnitudes in the upper part of the region. Some of the motion in the third direction is into the page, which is indicated by blue color. Green zone shows the extremely small components in out of plane direction.

5º Pitch: Figure 12 shows a dominant upwash behavior in the whole region, as expected. The radial velocity has almost the same magnitude across the region. However, in the region above the path of the blade, the radial components become more effective towards the rotor center. Besides, the negative pitch again appears to be an image pair of the positive pitch.

The negative pitch results seem to be reasonably symmetrical with respect to positive pitch results. This is again because of the almost symmetrical character of the airfoil. In a typical positive pitch experiment, the central area of the rotating blade system generates a strong downwash. However, some of the downwash area related fluid starts moving upward after impinging on the ground surface. Near the tip plane and in the outer region, an associated upward motion is very typical.

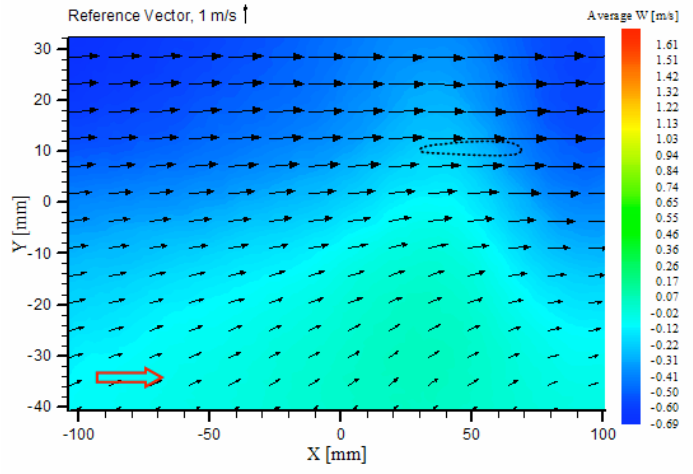

Figure 11. 3D vector map with colored contours at 0º pitch 3 cm (1.18 in) in front of the tip

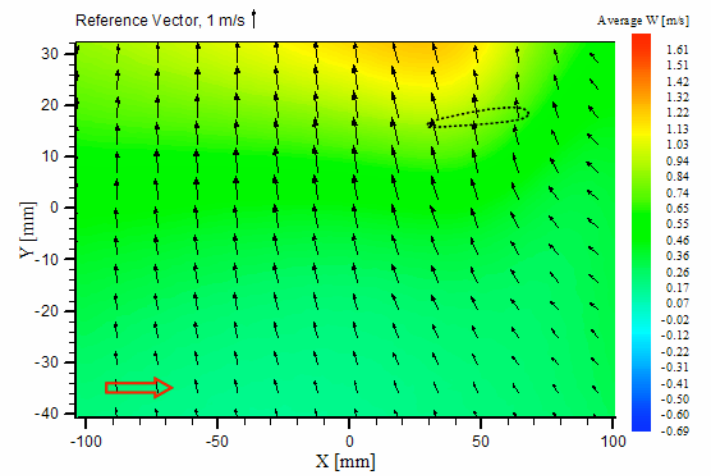

Figure 12. 3D vector map with colored contours at 5º pitch 3 cm (1.18 in) in front of the tip

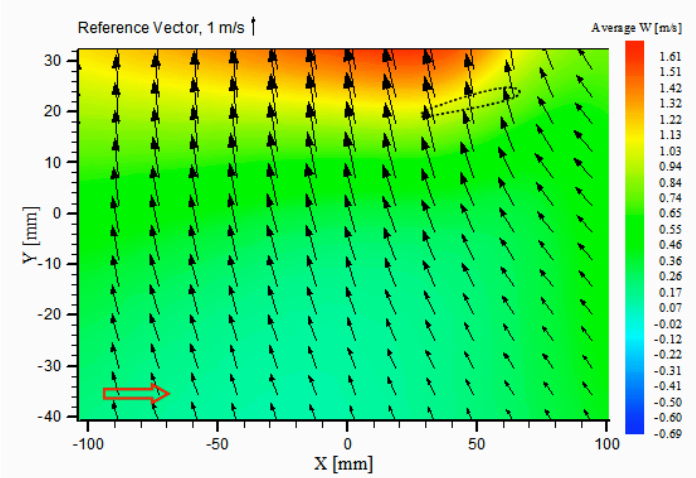

Figure 13. 3D vector map with colored contours at 10º pitch 3 cm (1.18 in) in front of the tip

10º Pitch: The upwash motion is more distinct for higher pitch as in Fig. 13. The radial components become more significant. The location of the blade is observed to be moving in the vertical axis again, as a result of a higher pitch applied to the blade.

CONCLUSIONS

A stereoscopic PIVsystem was used to obtain 3D flow field details near a helicopter blade tip. The results are obtained in phase-locked condition in rotating frames in order to investigate a fixed position.

The lift production of the blade for positive pitch values is obvious from the downwash behavior of the flow. For negative pitch case, this becomes upwash behavior as expected. The negative and positive pitch cases corresponding to the same values give results almost like a mirror image of one another due to the almost symmetric structure of the airfoil. The lift force acting on the blades can also be observed due to blades' elastic motion as a displacement of the airfoil in the vertical direction on the maps of 3D PIV results. For -5º, 0º, 5º, and 10º pitch, the airfoil is found to be located at around Y= 1 mm (0.04 in), 8 mm (0.31 in), 15 mm (0.59 in), and 22 mm (0.79 in), respectively.

For positive pitch case, it is observed that approximately 30 mm (1.18 in) below the airfoil, downwash behavior turns into a slight upwash motion. This upward flow may be due to the part of the flow reflecting from the ground, where the rotor blades are 132 cm (52 in) above the ground. This is a strong effect near the tip, hence it is not observed at the section further away from the tip. The ground effect decreases as the positive pitch amount is increased from 5º to 10º, as well. It is observed from the maps that the level where the flow is reflected from the ground gets closer to the surface for the higher positive pitch (Y=-36 mm (-1.42 in), approximately 58 mm (2.28 in) below the airfoil). This ground effect can be overcome by placing the helicopter blades higher above the ground.

At the further section away from the tip, for both positive and negative pitch cases, a clean boundary layer forms without the tip vortex generation felt at the tip. As a result, the velocity components on the upper and lower surfaces of the airfoil are reduced in magnitude. This is observed as a reduction of velocity magnitude, roughly from 5.5 m/s (18 ft/s) to 4 m/s (13.1ft/s) for -5º pitch case, and from 8 m/s (26.2 ft/s) to 6 m/s (19.7 ft/s) for 5º pitch case.

The wakes of the airfoils at different pitches and locations can be observed from the maps, too. The wake of the airfoil at 0º pitch is the slightest among the others.

The near tip flow does not have a strong 3D appearance at 3 cm in front of the tip. This is because the airfoil is small in size, and the velocity of the rotor is not high enough to be able to affect the flow in the vicinity of the airfoil.

The horizontal velocity components observed in negative and zero pitch cases are due to the viscous shear imposed by the airfoil tip. The downwash area related fluid at positive pitch is found to be moving upward in front of the tip after impinging on the ground. In the same way, the upwash area related fluid at negative pitch starts moving down in front of the tip.

The positioning accuracy of the technique needs to be improved in order to determine the exact point of interest on the 3D maps. The airfoil is initially positioned in a plane which is parallel to the laser sheet via some trigger delay, so that its location corresponding to the target plate would be known. But, this has resulted in having the blades in the captured PIV images. As a consequence, laser reflections existed on the images.

REFERENCES

[1] Lang, H., Morck, T., Woisetschlager, J., 2002, "Stereoscopic Particle Image Velocimetry in a Transonic Turbine Stage," Experiments in Fluids, **32**, pp. 700-709.

[2] Alkislar, M. B., Lourenco, L. M., Krothapalli, A., 2000, "Stereoscopic PIV Measurements of a Screeching Supersonic Jet," The Visualization Society of Japan and Ohmsha, Ltd., Journal of Visualization, **3**, No.2, 135-143.

[3] Hill, D. F., Sharp, K. V., Adrian, R. J., 2000, "Stereoscopic Particle Image Velocimetry Measurements of the Flow Around a Rushton Turbine," Experiments in Fluids, **29**, pp. 478-485, Springer-Verlag,.

[4] Funes-Gallanzi, M., Bryanston-Cross, P. J., Chana, K. S., 1994, "Wake Region Measurements of a Highly Three-Dimensional Nozzle Guide Vane Tested at DRA Pyestock Using Particle Image Velocimetry," International Gas Turbine and Aeroengine Congress and Exposition, Netherlands.

[5] Uzol, O., 2000, "Novel Concepts and Geometries as Alternatives to Conventional Circular Pin Fins for Gas Turbine Blade Cooling Applications," The Pennsylvania State University, University Park.

[6] Uzol, O., and Camci, C., 2001, "Aerodynamic Loss Characteristics of a Turbine Blade With Trailing Edge Coolant Ejection Part 2: External Aerodynamics, Total Pressure Losses and Predictions," ASME Journal of Turbomachinery, **123**, No. 2, pp. 249-257.

[7] Tajiri, K., 2003, "Implementation of a Stereoscopic Particle Image Velocimetry at the Exit of an Axial Flow Turbine," The Pennsylvania State University, University Park.

[8] Lorber, P. F., 1990, "Aerodynamic Results of a Pressure-Instrumented Model Rotor Test at the DNW," 46th Annual Forum of American Helicopter Society, Washington D.C.

[9] Yu, Y. H., Tung, C., Gallman, J., Schultz, K. J., Van Der Wall, B., Spiegel, P., Michea, B., 1993, "Aerodynamics and Acoustics of Rotor Blade-Vortex Interactions," AIAA 15th Aeroacoustics Conference, paper 93-4332, Long Beach, CA.

[10] Leishman, J. G., Baker, A., Coyne, A., 1996, "Measurements of Rotor Tip Vortices Using Three-Component Laser Doppler Velocimetry," Journal of the American Helicopter Society, **41**, No.4, pp. 342-353.

[11] Leishman, J. G., Bhagwat, M. J., 1999, "Correlation of Helicopter Rotor Tip Vortex Measurements," AIAA Journal.

[12] Leishman, J. G., 1998, "Measurements of the Aperiodic Wake of a Hovering Rotor," Experiments in Fluids, **25** pp. 352-361, Springer-Verlag.

[13] Han, Y. O., Leishman, J. G., Coyne, A. J., 1997, "Measurements of the Velocity and Turbulence Structure of a Rotor Tip Vortex," AIAA Journal, **35**, No. 3.

[14] Coyne, A. J., Bhagwat, M. J., Leishman, J. G., 1997, "Investigation Into the Rollup and Diffusion of Rotor Tip Vortices Using Laser Doppler Velocimetry," American Helicopter Society 53rd Annual Forum, Virginia Beach, VA.

[15] Raffel, M., Seelhorst, U., Willert, C., 1996, "Vortical Flow Structures at a Helicopter Rotor Model Measured by LDV and PIV," 22nd European Rotorcraft Forum, Brighton, UK.

[16] Saripalli, K. R., 1995, "Application of Particle Imaging Velocimetry Techniques to Helicopter Rotor Flowfields at McDonnell Douglas Aerospace," 33rd AIAA Aerospace Sciences Meeting and Exhibit, Reno.

[17] Horner, M. B., Stewart, J. N., Galbraith, R. A. McD., Grant, I., Coton, F. N., 1994, "An Examination of Vortex Deformation During Blade-Vortex Interaction Utilising Particle Image Velocimetry," 19th Congress of the International Council of the Aeronautical Sciences, **2**.

[18] Heineck, J. T., Yamauchi, G. K., Wadcock, A. J., Lourenco, L., Abrego, A. I., 2000, "Application of Three-Component PIV to a Hovering Rotor Wake," American Helicopter Society 56th Annual Forum, Virginia Beach, Virginia.

[19] Burley, C. L., Brooks, T. F., Van Der Wall, B., Richard, H., Raffel, M., Beaumier, P., Delrieux, Y., Lim, J. W., Yu, Y. H., Tung, C., Pengel, K., Mercker, E., 2003, "Rotor Wake Vortex Definition Using 3C-PIV Measurements – Corrected for Vortex Orientation," 9th AIAA/CEAS Aeroacoustics Conference, Hilton Head, South Carolina.

Adaptive Correlation			**5 cm (1.97 in) away from the tip**			**-5° pitch**	**0° pitch**	**5° pitch**	**10° pitch**
					Calibration	*Laser Setup*			
			Mode		_	Asynchronous	Asynchronous	Asynchronous	Asynchronous
#refinement steps		2	**Acqusition Control**	time between pulses	30000 μs	150 μs	200 μs	100 μs	100 μs
number of passes/step				burst start	user action from PC	External burst trigger	External burst trigger	External burst trigger	External burst trigger
initial step		1		trigger delay	–	14000.20 μs	14000.20 μs	14000.20 μs	14000.20 μs
intermediate step		1	**3 cm (1.18 in) in front of the tip**			**-5° pitch**	**0° pitch**	**5° pitch**	**10° pitch**
final step		1			*Calibration*	*Laser Setup*			
Moving-Average Validation			**Mode**		_	Asynchronous	Asynchronous	Asynchronous	Asynchronous
	averaging area	3x3	**Acqusition Control**	time between pulses	30000 μs	250 μs	200 μs	300 μs	250 μs
	acceptance factor	0.1		burst start	user action from PC	External burst trigger	External burst trigger	External burst trigger	External burst trigger
	iterations	3		trigger delay	–	14000.20 μs	14000.20 μs	14000.20 μs	14000.20 μs

Table 1. Calibration and Laser Setup Parameters